JCTC Journal of Chemical Theory and Computation

Article

pubs.acs.org/JCTC

Toward Reliable Prediction of the Energy Ladder in Multichromophoric Systems: A Benchmark Study on the FMO Light-Harvesting Complex

Nanna Holmgaard List,*[,†] Carles Curutchet,[‡] Stefan Knecht,[†,§] Benedetta Mennucci,[¶] and Jacob Kongsted*[,†]

[†]Department of Physics, Chemistry and Pharmacy, University of Southern Denmark, Campusvej 55, DK-5230 Odense M, Denmark

[‡]Departament de Fisicoquímica, Facultat de Farmàcia, Universitat de Barcelona, Av. Joan XXIII s/n, 08028 Barcelona, Spain

[§]Laboratory of Physical Chemistry, ETH Zürich, Wolfgang-Pauli-Straße 10, 8093 Zürich, Switzerland

[¶]Dipartimento di Chimica e Chimica Industriale, University of Pisa, Via Risorgimento 35, 56126 Pisa, Italy

Supporting Information

ABSTRACT: We present an evaluation of the performance of various single-reference QM methods for the prediction of the relative site energies and transition moments of the *Q* bands in the bacteriochlorophyll *a* (BChl *a*) pigments of the Fenna–Matthew–Olson (FMO) complex. We examine the relative merits of ZINDO, CIS, TD-DFT (with the functionals PBE, BLYP, PBE0, B3LYP, and CAM-B3LYP) and RI-CC2 in reproducing the variations across the pigments that occur as a consequence of geometrical and electrostatic effects of the FMO complex by comparison to DFT-BHLYP/MRCI. We find that these pigments are near-multiconfigurational in nature and, thus, constitute critical cases for the RI-CC2 method. The commonly used ZINDO method is fairly reliable for the site energies of the isolated pigments; however, it overestimates the coupling to the environment, thereby leading to variations across the embedded pigments that are too drastic. The overall best performance is provided by the investigated TD-DFT methods, where PBE0 is found to be slightly superior to the other functionals tested.

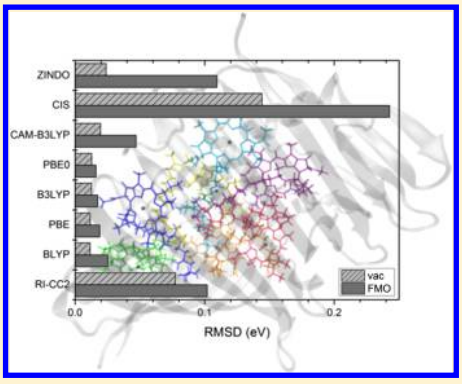

1. INTRODUCTION

In photosynthesis, sunlight is collected by a vast network of pigment molecules, appropriately arranged in pigment–protein complexes, and subsequently funneled through multiple electronic energy transfer (EET) reactions toward the reaction centers.[1−3] The high quantum efficiency of this light-harvesting process has inspired researchers for decades toward design of optimized artificial antennae.[4] An accurate theoretical description of such processes, which aims at relating spectroscopic observations and crystal structures, represents an important ongoing challenge expected to impact our ability to design novel materials with optimal light-harvesting properties.

Theoretical efforts are presently focused on two important aspects. First, the development of theories able to describe the dynamics of energy transfer in the intermediate coupling regime—an area that has attracted much attention since the recent discovery of long-lasting quantum coherence effects in pigment–protein complexes, a signature of such an elusive regime for EET.[5−11] This represents a situation where both the coupling between the electronic transitions of the pigments and the pigment–protein interactions should be treated on an equal footing.[12,13] The second main direction for the theoretical approaches consists of accurate estimation of the EET parameters needed in the modeling of the light-harvesting process: (i) the uncoupled electronic transition energies of the pigments (site energies), (ii) the electronic couplings between the pigments, and (iii) the spectral density of the pigment–protein coupling. Recent advances in quantum chemistry now allow quite robust calculations of electronic couplings, including the important screening effects induced by the surrounding environment.[14−19] An accurate estimation of site energies and spectral densities, however, is more challenging; so often, these parameters are obtained from a simultaneous fit of steady-state spectra and kinetic data.[20] Such strategy, however, becomes impractical when the number of pigments is large, as is often the case in photosynthetic complexes. Moreover, it does not provide any information on how the protein tunes the pigment energies in order to optimize the process and direct the captured energy toward the desired final trapping site.

An attractive strategy for the calculation of site energies relies on the application of combined quantum mechanics/molecular mechanics (QM/MM) methods, in which the pigments are described quantum-mechanically and the protein matrix

Received: June 29, 2013
Published: September 18, 2013

through a classical force-field.[21−25] A somewhat different approach is the electrostatic method developed by Renger and co-workers:[26,27] in such a method a real QM/MM method is not used but the solvatochromic shift is obtained by describing the ground and excited states of the pigments through partial charges derived from a given QM method.

When applying the QM/MM approaches, however, a natural question arises: how robust are these predictions with respect to the choice of QM or MM model? In the past decade, several groups have extensively benchmarked different QM methods for the estimation of electronic transition energies in organic chromophores,[28−35] and specifically for photosynthetic pigments such as chlorophylls and bacteriochlorophylls.[36] Overall, these studies indicate that pure functionals tend to be less consistent than hybrids in the context of time-dependent density functional theory (TD-DFT), giving rise to errors of the order of 0.2−0.3 eV. Semiempirical approaches or other cheap alternatives such as CIS are less accurate, whereas more expensive methods such as DFT/MRCI, CC3 or CASPT2 are more robust. Interestingly, such studies suggest that the performance of CC2 is similar to TD-DFT, despite its higher computational cost. When such methods are applied, for instance, to the determination of the relative energies of the chlorophylls in a complex, one can expect some cancellation of errors. However, it is unclear which error bars one could expect on the relative values of the site energies.

Recently, several groups have addressed the calculation of site energies in the Fenna−Matthews−Olson (FMO) complex of green sulfur bacteria using different flavors of QM/MM. The crystal structure of FMO was solved more than three decades ago, being the first known structure of a photosynthetic pigment−protein complex.[37] However, there is still controversy over the energetic ordering of the pigments, and different theoretical strategies predict somewhat different pictures of the overall energy ladder in FMO.[23,24,38] To illustrate the difficulty involved in such estimates, let us recall that the largest energy differences among the bacteriochlorophylls (BChls) in FMO amount to 400 cm^{-1} (0.05 eV), and this should be compared to the errors inherent to the QM and MM models of choice, but also in the set of geometries used for excited-state calculations. The latter problem is related to inaccuracies in the internal geometries of the pigments, typically extracted from the crystal or from classically based simulations, and it can be overcome adopting the electrostatic method proposed by Renger and co-workers.[26] However, this strategy neglects contributions to the relative site energies arising from slightly different conformations of the pigments in the protein scaffold, an effect that was recently suggested to be significant for site-energy tuning in the PE545 complex of cryptophytes.[25] We have also recently shown that explicit account of electronic polarization in the MM region can impact the solvatochromic shifts of the bilin pigments in PE545 in different ways,[39] thus suggesting that caution must be applied when site energies are estimated from simple nonpolarizable protein potentials constructed from fixed partial charges.

In this study, we investigate how the choice of the QM method impacts the estimation of relative site energies in the FMO complex. We intend to assess the reliability of different methods in accounting for energy differences among pigments that arise either from changes in conformation of the pigments or local pigment−protein interactions. To increase the transparency of the error sources we employ, for the purpose of the latter, a standard electrostatic embedding potential. We investigate the performance of several methods previously applied to FMO, such as TD-DFT, combined with a few commonly used functionals, and the semiempirical ZINDO method. In addition, we explore the behavior of configuration-interaction with single excitations (CIS), and also the more expensive alternatives; resolution of identity approximate second-order coupled cluster (RI-CC2) and the combined density functional theory/multireference configuration interaction (DFT/MRCI) method, which have previously been employed in the study of the absorption spectrum of chlorophyll *a*.[40,41] We focus our analysis on the relative merits of the methods in predicting the energies of the Q_y lowest excited state of BChl, which dictates the energy migration pathways and trapping site in the FMO complex. In the Supporting Information (SI), however, we include an analogous analysis for the Q_x excited state.

2. COMPUTATIONAL DETAILS

2.1. System Setup. The calculations in this study are based on the crystal structure of FMO from the green sulfur bacterium *Prosthecochloris aestuarii* (PDB ID: 3EOJ;[42] resolution = 1.3 Å). We restrict our analysis to the first seven BChls, since the eighth pigment, because of its peripheral location at the interface to the chromosome, would require a more extensive preparation of the crystal structure to obtain a realistic local environment. Protein preparation was performed using the Protein Preparation Wizard[43,44] implemented in the Schrödinger Suite 2011. The phytyl chain of some of the BChls is present in alternate conformations in the PDB file. We selected the coordinate set with the highest occupancies for each BChl. Waters beyond 5 Å from each BChl were removed. Several amino acid residues (1−6, 214) are missing in the PDB file. These have not been considered in this study. The gap in the polypeptide chain caused by the missing Glu214 was treated as follows. Gly213 was capped with H-atoms at the C_α atom since the C and O atom of Gly213 are missing. Similarly, Lys215 was truncated and capped at the C_α atom. The missing side chain of this residue was not modeled, because its inclusion would have introduced an unscreened charge in this region of the protein, because of the missing negatively charged Glu214. Although contributing with a negative charge, the side chain of Asp7 was not modeled, since its location is hardly predictable, because of its surface position and the missing neighbor residues at its N-terminal. This seems reasonable as this residue is located far from the BChls (∼13 Å from the nearest BChl). Modeling of the remaining missing side chains was accomplished using Prime 3.0[45−47] with default settings. Hydrogen atoms were added to the structure according to physiological pH. Thus, all Lys and Arg residues were positively charged while all Asp and Glu residues were negatively charged. Protonation states and tautomeric forms of His residues were determined using the Protein Assignment in the Protein Preparation Wizard. Apart from His12, all His residues were assumed to be neutral, and His227 and His297 were further assumed to adopt the ε-tautomeric form. The flip states of the Gln and Asn residues were examined, thereby leading to a flip of the side chain amide of Asn132, Asn135, Asn156, Asn206, Asn289, Asn305, and Asn334, as well as Gln167 and Gln263. Finally, the positions of the hydrogen atoms were optimized with the OPLS2005 force field[48] while keeping the heavy atoms fixed. The total charge of the prepared protein was −2.

2.2. Optimization. After having prepared the protein structure, we performed a QM/MM geometry optimization of

each BChl embedded in the FMO complex using the Qsite 5.7[49−51] module in the Schrödinger Suite. We followed a sequential optimization protocol; in each step, one of the monomers (starting from BChl 1 and proceeding up to BChl 7) was defined as the QM region while the remaining six BChls in the given step, together with the amino acids and water molecules, constituted the MM portion. The protocol was stopped after the first iteration through the pigments. The optimizations were conducted using the B3LYP[52−55] exchange-correlation functional in conjunction with the LACVP*[56] basis set on metals and the 6-31G*[57,58] basis set on all other atoms in the QM region. The MM region was represented by the OPLS2005 force field and the positions of the atoms included in this region were kept frozen in a given optimization step; that is, in the final optimized geometry of the FMO complex only the amino acids and crystallographic water molecules preserve the location from the crystal structure.

2.3. Electronic Structure Calculations. Vertical excitation energies and corresponding transition dipole moments of the Q_y electronic transition (and Q_x; see the SI) of the individual BChls were computed both in vacuum and embedded in the FMO complex using different QM methods (see below). Transition dipole moments were calculated in the dipole-length representation. The electrostatic embedding scheme was employed to account for effects of the protein environment by assigning to the atoms in the MM region charges taken from the OPLS2005 force field. To increase the efficiency of the computations, the BChls were terminated at the C4 atom and the dangling ends were capped with hydrogen atoms. The remaining part of the phytyl moiety and the six other BChls were included in the MM region. Point charges within 1.25 Å of the QM region (the hydrogen atoms bonded to the C5 atom of the phytyl tail) were removed.

2.3.1. DFT/MRCI. We used a parallelized version of the combined DFT/MRCI method[59,60] to compute the Q_y transition (and Q_x transition; see the SI), as well as the associated transition dipole moments of each BChl at their respective QM/MM DFT equilibrium geometries. The DFT/MRCI calculations were carried out using a split valence basis set with *d* polarization functions on all non-hydrogen atoms (def2-SV(P)).[61] The configuration state functions (CSFs) in the MRCI expansion were built from KS orbitals using the BHLYP[62,63] functional as implemented in Turbomole 6.3.[64] All 1s shells of the heavy first- and second-row atoms, as well as the 2s shell of Mg were kept frozen in the subsequent MRCI step, which corresponds to the default "freeze" option in Turbomole. The initial MRCI reference space was spanned by all single and double excitations from the eight highest occupied molecular orbitals (HOMOs) to the six lowest unoccupied molecular orbitals (LUMOs) of the ground-state KS determinant. In these preliminary calculations, an orbital selection threshold of $0.6E_h$ was employed and, in all cases, the 12 lowest roots were determined. The final reference space consisted of all configurations that contributed with a squared coefficient of at least 0.003 to one of the roots in the preceding initial DFT/MRCI run. In the production DFT/MRCI run, wave functions and excitation energies were computed for eight electronic states making use of a tighter selection threshold of $1.0E_h$, which follows the original recommendation by Grimme and Waletzke.[59]

2.3.2. RI-CC2. In addition to DFT/MRCI calculations, frozen core RI-CC2 calculations were carried out also using Turbomole. The poles and residues of the CC2 response function are correct through second and first order, respectively, in the fluctuation potential for transitions dominated by a promotion of a single electron.[65] Thus, we can expect the CC2 model to perform well for systems dominated by a single configuration and for excitations governed by single electron displacements. We employed Dunning's correlation-consistent double-ζ quality basis set augmented with diffuse functions (aug-cc-pVDZ) in combination with the corresponding optimized auxiliary basis set to treat the four-index electron repulsion integrals in the RI approximation.[66] The frozen orbital approximation was also applied in this case with the same settings as described above. As an indicative measure of the quality of the CC2 ground-state wave function, we employed the D_1 diagnostic test.[67]

2.3.3. DFT, CIS, and Semiempirical Methods. Finally, TD-DFT, CIS and ZINDO semiempirical calculations were performed using the Gaussian 09 package.[68] The ZINDO calculations were based on Zerner's spectroscopic parametrization,[69] whereas the TD-DFT calculations were performed using the following exchange-correlation functionals: the GGA (generalized gradient approximation) functionals BLYP[62,70] and PBE,[71] the hybrid functionals B3LYP and PBE0,[72] in addition to the long-range corrected CAM-B3LYP functional.[73] In the CIS and TD-DFT calculations, core orbitals were excluded from the active space, whereas all orbitals were included in the ZINDO calculations, according to Gaussian 09 defaults. When appropriate, the protein background charges were included in the calculations through the charge keyword.

3. RESULTS AND DISCUSSION

3.1. DFT/MRCI Reference. The DFT/MRCI approach is a genuine multireference method that has shown to be a quite accurate—with errors of <0.2 eV for organic systems, relative to high-level ab initio methods[29]—and reliable approach to study the ground and excited states of extended π chromophores, including also chlorophylls.[40,74−76] In the present case, we find DFT/MRCI to provide excitation energies of the Q transitions of the BChls within 0.1 eV of the experimental values reported by Louwe et al.[77]

To assess the suitability of the various single-reference approaches to provide an appropriate description of the ground state and Q_y excited state of the BChls, we briefly characterize the states of interest based on the benchmark DFT/MRCI data. According to our calculations (see Table 1), the ground state of each BChl, both isolated and embedded in the protein, comprises besides the leading KS determinant (86%) equally

Table 1. Weight of the Main Configurations (Larger than 1%) in the Ground and First Excited State (Q_y) Wave Functions of the Isolated BChls[a]

state	SE	DE	main configurations
GS	0.2	12.6	86% GS 2% $\pi^2_{HOMO} \rightarrow \pi^2_{LUMO}$ 2% $\pi_{HOMO-1}\,\pi_{HOMO} \rightarrow \pi_{LUMO}\,\pi_{LUMO+1}$ 1% $\pi^2_{HOMO-1} \rightarrow \pi^2_{LUMO}$
Q_y	83.0	10.6	75% $\pi_{HOMO} \rightarrow \pi_{LUMO}$ 6% $\pi_{HOMO-1} \rightarrow \pi_{LUMO+1}$ 1% $\pi_{HOMO-7/HOMO-8}\,\pi_{HOMO} \rightarrow \pi^2_{LUMO}$

[a]Total single and double excitation contributions (in percentage), SE and DE, respectively.

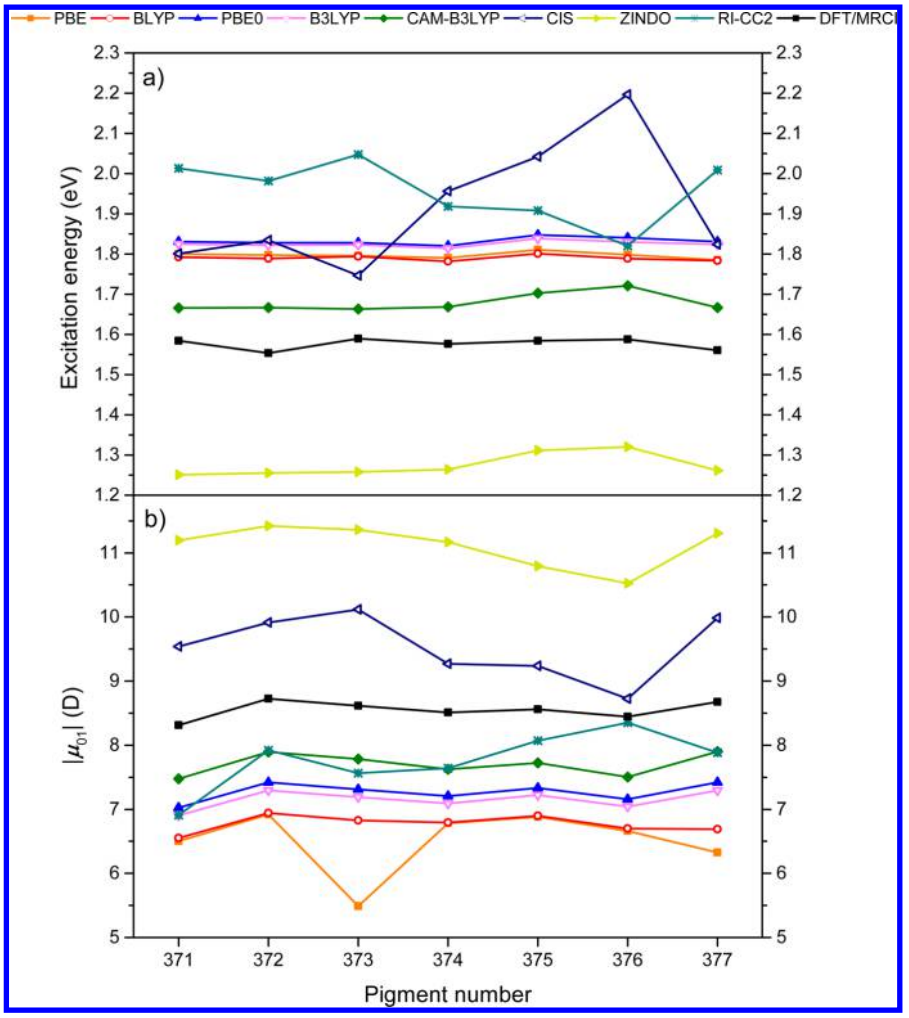

Figure 1. Comparison of (a) the Q_y excitation energies and (b) the Q_y transition dipole lengths of the seven isolated BChl pigment models obtained at different levels of theory. State mixing is observed for BChl 373 and BChl 377, using the PBE functional.

important, non-negligible contributions from double excitations (~13%). Singly excited configurations, on the other hand, play only a minor role. Turning to the Q_y transition in the isolated BChl pigments, we find that this excitation is mainly governed by a single excitation from HOMO into LUMO (75%). Further non-negligible contributions stem from a single excitation out of HOMO-1 into LUMO+1 and the double excitation out of HOMO-7/8 and HOMO into LUMO. Embedding the pigments in the point charge environment of the protein yields a significant change in the composition of the excited-state wave function, particularly, for BChl 6 (vide infra) where the double excitation from HOMO-1 and HOMO into LUMO and LUMO+1, as well as the ground-state KS determinant now contribute with a weight of 1%−1.5% each.

As gauged by the amount of double excitation character in their ground-state wave functions, the BChls in FMO are borderline to representing actual multireference problems; therefore, these pigments may pose a difficulty for single-reference QM methods. To assess the ability of the single-reference methods under consideration to reproduce the relative site energies across the pigments, we shall use the root-mean-square deviation (RMSD) with respect to DFT/MRCI defined as

$$\mathrm{RMSD} = \sqrt{\frac{1}{N}\sum_{i=1}(\Delta x_i - \bar{x})^2} \quad (1)$$

where the summation runs over pigments, N is the total number of pigments, and $\Delta x_i = x_i^Y - x_i^{\mathrm{ref}}$ the difference between the excitation energy for pigment i at the QM level Y and the DFT/MRCI reference, while $\bar{x}$ is the corresponding mean error over all pigments.

3.2. Isolated Pigments. We begin by examining the impact of the structural variations among the pigments on the relative performances of the considered theoretical methods. Figure 1a displays the Q_y excitation energies for the seven isolated pigments computed at different levels of theory. A first inspection of the results obtained at the DFT/MRCI level reveals that the transition energies are not very sensitive to the particular conformation adopted by the pigment (the variations range from 0.002 eV to 0.04 eV). Such small differences, however, turn out to be relevant, given that optical spectra suggest that the BChl energies span a range from ~0.05 eV in the FMO complex.[78] Thus, as already noted, to assess the relative site energetic ordering of the pigments even at the qualitative level, we must be able to discriminate these small energy differences between the pigments.

As illustrated in Figure 1a, the trends in vacuum site energies across the seven pigments obtained with the different single-

reference QM methods vary significantly. The CIS method provides a picture across the pigments that not only strongly exaggerates the differences between the pigments induced by the geometrical variations but also completely fails to capture the trend in relative site energies compared to the DFT/MRCI reference. To further understand this discrepancy, we computed the differences between the ground-state and excited-state Mulliken charges using CIS and compared them to those obtained with DFT/MRCI. The differential charges predicted by CIS and DFT/MRCI are shown in Figure S1 in the SI. Based on this comparison, we find that CIS significantly overestimates the charge rearrangement upon excitation. In addition, the charge redistribution at the CIS level is, contrary to DFT/MRCI, strongly dependent on the conformation of the pigment. This clearly illustrates that CIS provides an inadequate description of the nature of the excitation, and, thus, it is incapable of reproducing the spectral variations in the Q_y excitation across the pigments. This is also in accordance with previous work[22] on the BChls of light-harvesting complex II, where CIS was found to provide substantially larger variations in excitation energies along an MD trajectory, compared to B3LYP and ZINDO.

In moving to RI-CC2, the agreement with DFT/MRCI does not improve significantly; in fact, the RI-CC2 results do not follow any obvious pattern. While the trend in relative site energies for BChls 371−373 seems to be in qualitative agreement with that of the DFT/MRCI reference, we observe a deviating behavior across the remaining pigments. A similar grouping of the pigments emerges from the D_1 diagnostics listed in Table 2; BChls 371−373 and 377 exhibit a significantly

Table 2. D_1 Diagnostics for the RI-CC2 Ground-State Wave Functions of the Seven Pigments in Vacuum and in the Point Charge Environment of the FMO Complex[a]

	vacuum		in-protein	
BChl	D_1	$\langle\bar{E}_1\|E_1\rangle$ (%)	D_1	$\langle\bar{E}_1\|E_1\rangle$ (%)
371	0.1593	85.27	0.2025	84.93
372	0.1956	85.96	0.2707	84.10
373	0.0993	85.09	0.1916	85.19
374	0.2765	84.36	0.3110	83.74
375	0.2965	84.22	0.3294	83.49
376	0.3394	83.45	0.3463	82.80
377	0.1803	85.34	0.2621	84.42

[a]The biorthogonal overlap $\langle\bar{E}_1|E_1\rangle$ gives the percentage of single excitations, contributing to the Q_y transition.

smaller D_1 value (0.1−0.2), compared to the other pigments (∼0.3). While the D_1 values of the first set of pigments lie within or slightly above the acceptable range, the values for remaining pigments are far beyond the recommended value (D_1 = 0.10−0.15).[79] Above that, the Q_y excited state is characterized by notable double excitation contributions, which exceed 14% for all pigments (Table 2), in accord with the DFT/MRCI description in Table 1. Despite that the D_1 diagnostic also (and largely) reflects the degree of orbital relaxation and thus is not an unambiguous measure of the quality of the RI-CC2 wave function, these high D_1 values, taken together with the large percentage of double-excitation character, lead us to conclude that RI-CC2 is ill-suited for describing the considered multichromophoric system.

In contrast, we find that TD-DFT combined with the different functionals provide results in overall reasonable agreement with the trend of the DFT/MRCI reference. To highlight the relative performances of the xc-functionals, a focused view on only these methods is provided in Figure S8a in the SI. The considered GGA and hybrid functionals give virtually the same trend in site energies across the pigments and also on the absolute scale, the two classes of functionals provide similar Q_y excitation energies (i.e., the GGA results are within 0.05 eV of those produced by the hybrids). However, note that, in some cases (BChl 373 and BChl 377), the PBE results are affected by state mixing, as seen clearly from the diverging behavior for the transition moments (see below). Interestingly, the GGA and hybrid functionals have a tendency to downscale the differences in excitation energies induced by the structural changes in the BChl molecules, compared to those of the DFT/MRCI reference, despite the fact that the spread in differential Mulliken charge profiles across the pigments is larger for B3LYP than DFT/MRCI (see Figure S1 in the SI). The main differences concern the incorrect ordering of the site energies of BChl 375 and BChl 376 and the missing drop in the site energy of BChl 372. Actually, the latter represents the largest energy difference (ca. 0.04 eV) between the pigments at the DFT/MRCI level of theory. The site energies obtained using the hybrid (and GGA) functionals tend to exceed the DFT/MRCI counterparts, as previously reported.[29] Turning to the long-range corrected CAM-B3LYP functional, the order in energy of BChl 375 and BChl 376 is now qualitatively reproduced but the energy gap is overestimated, relative to the DFT/MRCI counterpart. Like the GGA and hybrid functionals, CAM-B3LYP does not capture the decrease in the site energy of BChl 372 and seems to have a slightly larger propensity than the other two classes of functionals to smoothen out the small features found in the relative energies predicted by DFT/MRCI. Overall, CAM-B3LYP therefore displays slightly larger deviations from the DFT/MRCI results than the other functionals. We also note that, contrary to the general trend, the CAM-B3LYP Q_y transition energies are consistently ∼0.2 eV below those obtained using the hybrid functionals, while ca. 0.1 eV above the DFT/MRCI reference values. On the other hand, the transition energies obtained using the semiempirical ZINDO method are, as expected, significantly underestimated, however, ZINDO shows a reasonable trend across the pigments, and interestingly, the picture is very similar to the one provided by CAM-B3LYP.

To recapitulate the above analysis of the relative performances in predicting the trend in vacuum site energies, in Figure 4a (shown later in this work), we report the corresponding RMSDs for the different QM methods considered relative to the DFT/MRCI reference. This clearly shows the superior behavior of TD-DFT in combination with the five functionals investigated here. The best performances, with respect to DFT/MRCI, are obtained using the GGA and hybrid functionals; however, it should be kept in mind that, for some of the isolated BChls, PBE leads to admixture of states. The CAM-B3LYP functional is less efficient and is only a slight improvement over ZINDO.

We continue to assess the performances with respect to the transition dipole moments associated with the Q_y excitation. The excitonic couplings between the pigments exhibit a first-order dependence, not only on the magnitude of the transition dipoles of the individual pigments but also on their relative orientation in the chromophores. However, since the trends in relative performances of the different theoretical methods are similar for the individual components of the transition dipoles,

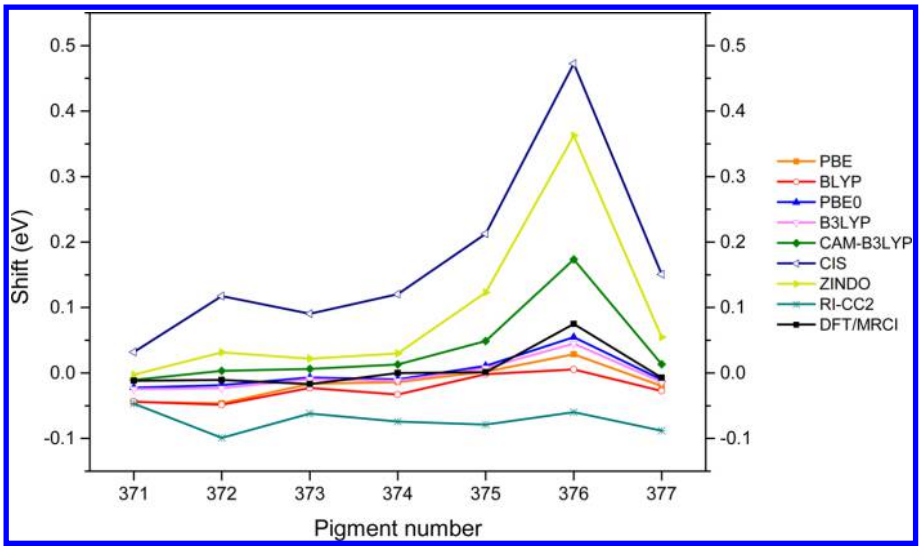

Figure 2. Shifts in Q_y excitation energy upon inclusion of the point charge environment of the protein for the seven BChl pigment models provided by the different treatments of the QM region.

we will, for the sake of brevity, henceforth restrict ourselves to the discussion of the transition dipole lengths. The Q_y transition moments in vacuum computed with the different methods are reported in Figure 1b. Moreover, a quantitative overview of the relative performances in terms of RMSDs is provided later in this work in Figure 4b.

First, by comparing Figures 1a and 1b, we note the tendency of an inverse relation between the site energies and the associated transition moments generally found for all methods. That is, a relatively higher site energy is associated with a comparatively lower transition dipole moment (compare, e.g., the behavior of BChl 371 and BChl 376 for DFT/MRCI). Assuming a simple particle-in-a-box model, this may be explained in terms of the degree of planarity of the BChl molecules and the resulting conjugation. Second, as seen in Figure 1b, the overall trends established in the previous paragraph for the excitation energies are largely transferable to the transition dipole moments. The considerable discrepancies and unsystematic behavior observed for RI-CC2 are not unexpected recalling that the BChl molecules clearly constitute difficult cases for the CC2 model, as discussed above. As found for the site energies, the trends provided by CIS for transition dipole moments are inconsistent with those obtained using DFT/MRCI. In accordance with the site energies, the DFT/MRCI trend in transition moments is captured well by most of the investigated DFT functionals (see Figure S8b in the SI for a picture including only the TD-DFT methods). However, the PBE results for BChl 373 and BChl 377 diverge from those obtained using the other functionals due to a slight mixing to an artificial state. Such mixing, however, does not significantly affect their site energies, which are in good agreement with the results obtained using the other functionals (see Figure S8a in the SI). In terms of dipole moments, the two hybrid functionals provide a picture across the pigments in very good agreement with the reference, despite that the differences due to the structural fluctuations in BChls 374−377 are mildly amplified. The two functionals yield almost identical absolute transition dipole lengths that are close to a previously reported value computed using the hybrid B3PW91 functional.[80] Apart from the divergent behavior at site 373 and 377 at the PBE level, which arises from the state-mixing issue discussed above, the GGA functionals provide trends similar to those of the hybrids. The trend obtained by means of CAM-B3LYP differs overall slightly more than the hybrids from the DFT/MRCI reference counterpart. Whereas the trend in the transition dipoles for the BChls 371−373 is, as opposed to that of the corresponding site energies, correctly reproduced, the larger discrepancy can be related to the slightly overemphasized fluctuations for BChl 376 and BChl 377. As previously noted, ZINDO outperforms CIS; however, its performance is much less convincing when it comes to the trends in transition dipole moments. Most notably, an erroneous decrease is predicted for BChl 375.

As summarized later in Figure 4b, we also conclude that, for the transition dipole moments of the isolated pigments, the two hybrid functionals B3LYP and PBE0 behave clearly better than the other considered methods.

3.3. Pigments Embedded in the Protein. Having discussed the results related to the isolated BChls, in this section, we continue to consider the relative merits of the different QM methods when including the effects of the surrounding environment. The Q_y excitation energies of the seven pigments embedded in the FMO complex are shown later in this work in Figure 3a. However, prior to considering these, it is instructive to assess the extent to which the pigments are modulated by the electrostatic interactions with the environment.

The shifts of the Q_y excitation energies in going from vacuum to inside the protein, obtained with the different methods, are provided in Figure 2 (see Figure S9 in the SI for the picture comparing only the TD-DFT methods). As evident from the shifts predicted by DFT/MRCI, the effect of introducing the point charge environment of the FMO complex is generally rather limited. That is, with the exception of BChl 376, the excitation energies of all pigments are only slightly altered (changes are <0.02 eV) upon inclusion of the protein environment and for all pigments but BChl 375 and BChl 376, the environment gives rise to a red-shifted transition energy. BChl 376 clearly marks a special case for which the increase of the excitation energy is more pronounced (0.075 eV), compared to the rest of the pigments. As discussed in previous studies,[81,82] this more pronounced blue-shift can be rationalized on the basis of the local environment surrounding

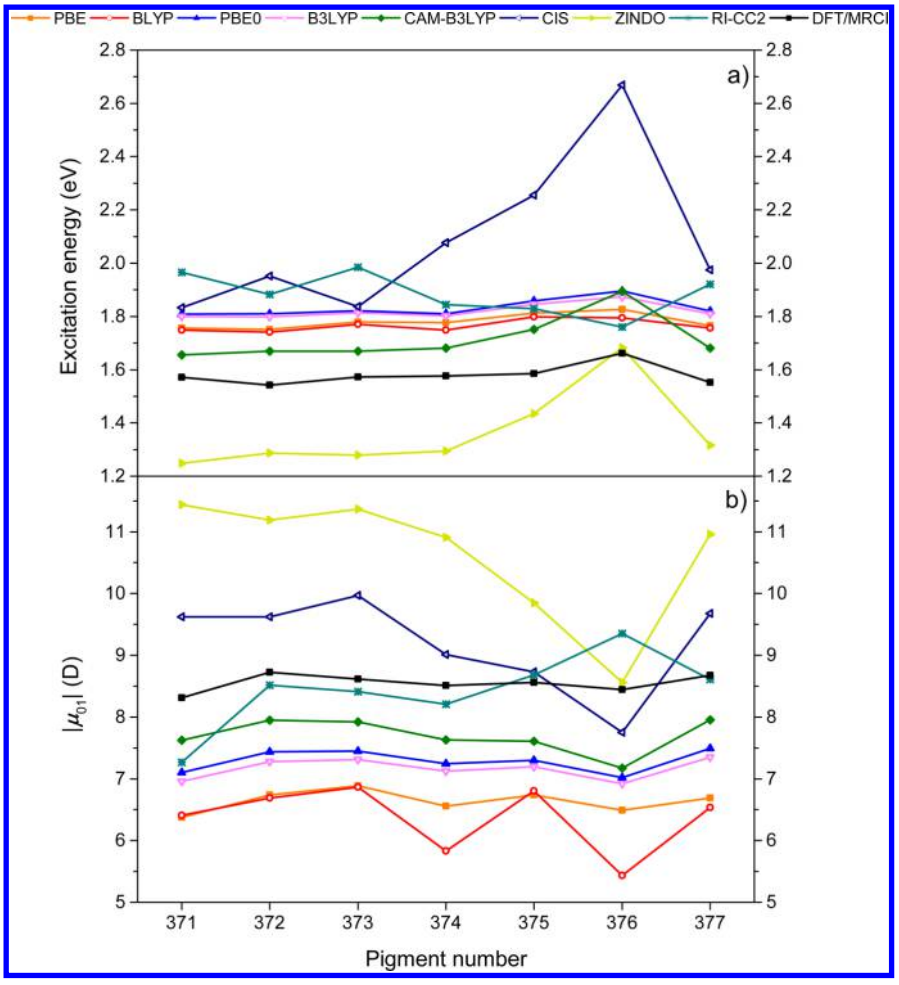

Figure 3. Comparison of (a) the Q_y excitation energies and (b) the Q_y transition dipole lengths of the BChl pigment models when placed in the protein environment computed at different levels of theory. State mixing is observed for BChl 374 and BChl 376, using the BLYP functional.

this pigment. Particularly, the Arg95 residue that acts as a hydrogen bond donor to the carbonyl group of the additionally fused ring of BChl 376 has been recognized as being mainly responsible for the observed blue-shift. In qualitative terms, this positively charged amino acid produces an electric field along the line connecting the nitrogens of the two unreduced pyrrole rings, which is pointing in the opposite direction of the transition dipole vector of the Q_y excitation. The environment thus destabilizes the excited state of this pigment with respect to its ground state, which explains the observed increase of the excitation energy for BChl 376 inside the protein.

Next, we turn to Figure 3a, which displays the trends in excitation energies of the embedded pigments for the considered methods. To clarify the trends across the different TD-DFT methods, Figure S10a in the SI displays a comparison between these methods and the DFT/MRCI reference. Contrary to DFT/MRCI, the CIS method predicts a blue-shift of the Q_y excitation energy for all pigments (Figure 2), and the differences between the pigments, which are already overemphasized in vacuum, become even more strongly amplified compared to the reference when taking into account the environment. This picture is consistent with the over-estimated differential Mulliken charges predicted in vacuum and inside the FMO complex (see Figure S1 in the SI), which lead to an artificial enhancement of the interactions between the pigments and the environment. Furthermore, as anticipated on the basis of its charged environment, the largest exaggeration is found for BChl 376. At the RI-CC2 level, on the other hand, all excitation energies are down-shifted compared to vacuum and no specific behavior is observed for BChl 376. In light of the questionable validity of the RI-CC2 method already found for the isolated pigments, the erratic behavior also seen when incorporating the environmental effects is not unexpected; indeed, the environment leads to even higher D_1 values (0.2−0.35). In accord with the vacuum results, the trends resulting from the application of the two hybrid functionals nearly coincide and are close to the DFT/MRCI counterpart, with the largest deviations at sites 372, 375, and 377, where the site energies are overestimated, with respect to that of BChl 371. Use of the GGA functionals slightly improves the hump at BChl 372, but at the expense of a poorer performance for BChl 376. In contrast to vacuum, in this case, the BLYP functional leads to some state-mixing for sites 374 and 376, whereas PBE only predicts some minor mixing in site 376. The overall trend across the seven pigments obtained with CAM-B3LYP follows roughly the reference; however, with the exception of BChl 371, all excitation energies are mildly blue-shifted (Figure 2). Moreover, the results for BChl 375 and BChl 376 seem to worsen relative to the hybrids. As in vacuum, the ZINDO method performs somewhat similar to CAM-B3LYP but with considerably larger deviations for BChl 375 and BChl 376. We also note that the trend for BChl 376

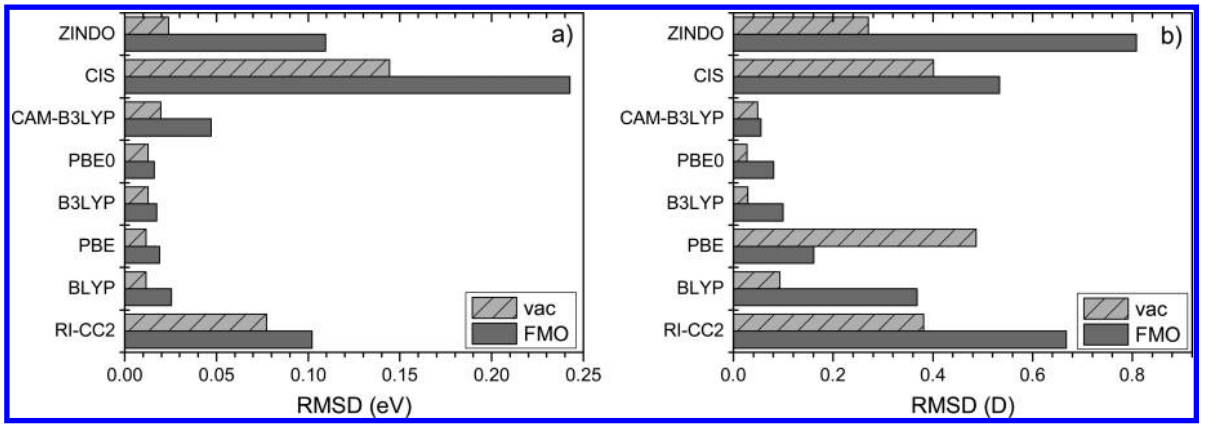

Figure 4. RMSDs as defined in eq 1 for (a) the Q_y excitation energies and (b) the Q_y transition dipole lengths in vacuum and placed in the protein environment obtained using the different methods.

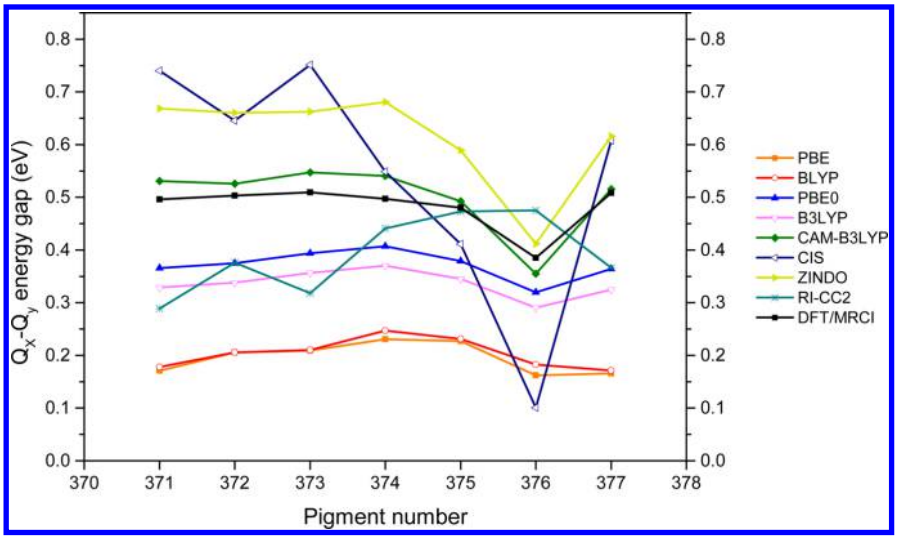

Figure 5. Energy difference between the Q_x and Q_y states of the seven embedded BChl pigment models obtained at different levels of theory.

obtained along the sequence BLYP−B3LYP−CAM-B3LYP−ZINDO suggests that the shift in the Q_y excitation energy of this pigment induced by the protein environment is particularly sensitive to the amount of exact exchange.

The above analysis is quantified in terms of the RMSDs in Figure 4a. These clearly illustrate that the conclusions regarding the relative performances of the different methods drawn for the isolated pigments largely hold when including the point charge environment of the protein. Most importantly, the PBE0 functional (and almost equally well B3LYP) exhibits the closest agreement with DFT/MRCI. We also note the additional complexity related to the inclusion of the direct environmental aspects. As apparent from Figure 4a, the differences between the considered theoretical methods and the reference are intensified when the pigments are placed in the environment.

Finally, turning to the length of the Q_y transition dipole moments for the embedded pigments, an overall picture similar to that obtained in vacuum emerges, as shown in Figure 3b. Particularly, we remark that the absolute transition dipole strengths across the pigments are only affected to a modest degree (except for BChl 376) by the electrostatic effects of the environment. The absolute values obtained using the hybrid functionals are closest to (ca. 1 D above) the experimental results obtained in monomeric solutions,[83−87] while, consistent with previous results,[29] the DFT/MRCI values are above those of B3LYP (by ∼1.5 D). The difficulty for the applied methods to correctly describe the interactions between BChl 376 (and BChl 375) and its environment found for the site energies is also manifested in the transition moments. Consistent with the trend in the corresponding site energies, the performance of CAM-B3LYP with regard to transition moments is only slightly impaired for these pigments, and thus, the overall picture is in reasonable agreement with DFT/MRCI. For a focused comparison of the relative performances of the different xc-functionals, we refer to Figure S10b in the SI. Again, the state-mixing issue, present for sites 374 and 376 using BLYP, impairs the prediction of the transition moments. ZINDO predicts far too drastic changes mediated by the environment and is incapable of capturing the trend across the pigments, even at the qualitative level. As expected on the basis of previous studies,[83−85,88] also the absolute transition dipole strengths provided by ZINDO are overestimated by almost a factor of 2. Once again, the best performance, with respect to DFT/MRCI, is obtained using the hybrid functionals, and as evident from the RMSDs depicted in Figure 4b, the DFT/MRCI results are generally better reproduced with PBE0, compared to B3LYP.

To summarize, we conclude that the two hybrid functionals provide the best compromise, with respect to DFT/MRCI among the applied methods for predictions of the trend in Q_y site energies across the pigments, both isolated and embedded

dx.doi.org/10.1021/ct400560m | J. Chem. Theory Comput. 2013, 9, 4928−4938

in the FMO complex. Particularly, the issue of state-mixing present when using the pure DFT functionals is remedied upon inclusion of exact exchange. The irregular behavior of RI-CC2 indicates that CC2 is much more sensitive than TD-DFT to the near-multiconfigurational nature and double-excitation contributions characterizing the electronic states of the considered pigments and offers no general reliable description in the present cases.

Finally, we briefly comment on the performance of the various QM methods to predict the Q_x-Q_y energy gap. As shown in Figure 5 for the embedded pigments (for the isolated pigments, see Figure S7 in the SI), the energy gaps estimated by DFT/MRCI and CAM-B3LYP are similar and also within the same range as the experimentally measured values in the FMO complex (i.e., including excitonic coupling) as well as in different monomeric solutions.[84,85,89] On the other hand, the GGA and hybrid functionals underestimate the energy separation between the two Q bands (by ∼0.33 and 0.15 eV, respectively), whereas ZINDO produces a too large energy difference, as consistent with previous work.[90] However, again inspecting the ability of the various methods in predicting the variations in the Q_x-Q_y energy gap across the different pigments, we find that these variations are equally well described by CAM-B3LYP and the hybrid functionals. Indeed, the calculated RMSDs, with respect to the DFT/MRCI reference, are found to be 0.025/0.027 eV (PBE0/B3LYP) and 0.023 eV (CAM-B3LYP), whereas the performance of the two GGA functionals is slightly worse 0.038/0.043 eV (PBE/BLYP). Thus, despite the better performance of CAM-B3LYP, with respect to the absolute value of the energy gap, this functional does not offer a significant improvement concerning the relative Q_x-Q_y gap across the pigments.

3.4. Comparison to Experiments and Previous Theoretical Results. During the last two decades, several groups have addressed the estimation of site energies in FMO, either from empirical fittings[91] or based on a classical[23,24,38] or a quantum-mechanical description of the surrounding protein environment.[78] The scope of the present study is not the quantitative estimation of the site energies in FMO, but rather assessing the reliability of different QM methods in accounting for site energy differences arising either from changes in pigment conformation or local pigment−protein interactions. A complete quantitative estimate of the site energies would involve further considerations, for example, inclusion of the entire phytyl chain and the fifth (sixth) ligand in the QM region, protein flexibility, and electronic polarization. Nevertheless, it is interesting to compare the site energies obtained from the present QM/MM calculations with previous studies. As already pointed out, the variations in the site energies are amplified when embedding the pigments in the FMO complex, and as judged from the present QM/MM results, the span of energies is very sensitive to the choice of QM method: ∼0.08 eV for PBE0 and B3LYP TD-DFT calculations, ∼0.12 eV for DFT/MRCI, and much larger values from the other methodologies. Such ranges are clearly too large, compared to other sets of site energies that were able to describe the absorption spectra of FMO, which span a range of ca. 0.05 eV.[78,91] However, it must be noted that, if we remove BChl 376 from our sets of energies, the range of values decreases to ca. 0.04−0.05 eV for PBE0, B3LYP, and DFT/MRCI. The large blue shift in BChl 376 found in some of our calculations, which is already apparent in some vacuum calculations, can thus be related to the geometry adopted by the pigment in our optimization, as well as to its resulting orientation relative to Arg95. Accounting for protein flexibility would most probably avoid such a problem. If this energy is excluded, PBE0, B3LYP, and DFT/MRCI provide a range of energies in good accord with previous studies, whereas the other methods here investigated perform significantly worse, spanning ranges >0.1 eV. These results support our conclusions, i.e., that TD-PBE0, TD-B3LYP and DFT/MRCI methods perform significantly better than the other methods in the estimation of relative site energies.

On the other hand, our results indicate that BChl 375 and BChl 376 have the largest site energies among the pigments. This is in agreement with the most widely accepted models of site energies in FMO derived theoretically[38] or from empirical fittings.[92] In addition, such models indicate BChl 373 as the energy sink in the complex, while in the present QM/MM calculations, the lowest energy site alternates between BChl 371 and BChl 372. Again, this disagreement might also be due to the neglect of protein dynamics. In fact, ref 23 indicates that the energy of BChl 373 was 0.05 eV higher than the lowest energy site in calculations based on the crystal structure, whereas accounting for protein flexibility through MD simulations reduced that gap to 0.02 eV.

4. CONCLUSIONS

In this paper, we have examined the accuracy of various single-reference quantum mechanical (QM) methods for the prediction of the relative site energies and associated transition moments of the Q bands in the BChl *a* pigments of the FMO complex by comparing to the combined DFT/MRCI approach.

From the analysis of the electronic states of the pigments obtained with the DFT/MRCI reference, we find the ground states of the pigments to be near-multiconfigurational in nature. Therefore, it is not surprising that the use of the RI-CC2 method leads to even qualitatively inconsistent results across the pigments. The TD-DFT methods, on the other hand, seem more robust to the multireference character and constitute the best choice among the considered methods for studying the variations among the Q transition energies and moments of the pigment molecules in FMO. Particularly, PBE0 provides, overall, the smallest deviations from the DFT/MRCI reference, however, closely followed by the B3LYP and CAM-B3LYP functionals. The pure DFT functionals PBE and BLYP, on the other hand, are less robust, because of occasional mixing of the states of interest with close-lying artificial states. The commonly used semiempirical ZINDO method provides reasonable trends for the isolated pigments, while, upon inclusion of the electrostatic effects of the protein, the variations in site energies, particularly for BChl 375 and BChl 376, are exaggerated. The CIS method does not properly account for the nature of the Q excitations, and, for the isolated pigments, already leads to incorrect trends across the BChls in FMO. This erroneous description of the excitations produces too strong couplings to the environment such that the erratic behavior is amplified further for the embedded pigments.

The results presented in this work clearly underline that relative methodological performances based on vacuum studies cannot be expected to be transferable to cases where coupling to an environment is included. Overall, our results indicate that TD-DFT methods based on hybrid functionals are better suited for the prediction of site energies in photosynthetic pigment−protein complexes than other popular choices such as CIS or semiempirical ZINDO calculations. This conclusion is in line

with previous benchmark studies assessing the relative merits of these methods in the determination of electronic transition energies. However, whereas typical error bars for TD-DFT energies are about 0.2−0.3 eV, we find that relative site energies can be determined to an accuracy of about 0.02 eV. This value suggests an approximate error bar for current models of predicted site energies, which can be useful when developing quantitative models of light harvesting.

■ ASSOCIATED CONTENT

Supporting Information

Mulliken population analysis of the Q_y transition in the isolated and embedded pigments. Comparison of the site energies and transition moments for the Q_x excitation calculated using the different QM models. Figures displaying a focused comparison of the relative performances of the investigated TD-DFT methods with respect to DFT/MRCI for the Q_y transition. This material is available free of charge via the Internet at http://pubs.acs.org/.

■ AUTHOR INFORMATION

Corresponding Author

*E-mail: nhl@sdu.dk (N.H.L.), kongsted@sdu.dk (J.K.).

Notes

The authors declare no competing financial interest.

■ ACKNOWLEDGMENTS

N.H.L. and J.K. thank the Lundbeck Foundation for financial support. B.M. acknowledges the European Research Council (ERC) for financial support in the framework of the Starting Grant (EnLight -277755). C.C. acknowledges support from the Ministerio de Economía y Competitividad of Spain (grants CTQ2012-36195 and RYC2011-08918) and computational resources provided by the Centre de Supercomputació de Catalunya. J.K. thanks the Danish Natural Science Research Council/The Danish Councils for Independent Research, the Sapere Aude programme and the Villum Foundation for financial support. S.K. acknowledges the Danish Natural Science Research Council for an individual postdoctoral grant (10-082944) and Prof. M. Reiher at ETH Zürich for financial support. S.K. is grateful to Prof. S. Grimme. Prof. C. M. Marian and Dr. M. Kleinschmidt for providing access to their parallelized DFT/MRCI code. The authors thank the Danish Center for Scientific Computing for computational resources.

■ REFERENCES

(1) Cheng, Y.-C.; Fleming, G. R. *Annu. Rev. Phys. Chem.* **2009**, *60*, 241−262.
(2) Collini, E.; Curutchet, C.; Mirkovic, T.; Scholes, G. D. In *Energy Transfer Dynamics in Biomaterial Systems*; Burghardt, I., May, V., Micha, D. A., Bittner, E. R., Eds.; Springer: Berlin, 2009; pp 3−34.
(3) Novoderezhkin, V. I.; van Grondelle, R. *Phys. Chem. Chem. Phys.* **2010**, *12*, 7352−7365.
(4) Scholes, G. D.; Fleming, G. R.; Olaya-Castro, A.; van Grondelle, R. *Nat. Chem.* **2011**, *3*, 763−774.
(5) Engel, G. S.; Calhoun, T. R.; Read, E. L.; Ahn, T.-K.; Mančal, T.; Cheng, Y.-C.; Blankenship, R. E.; Fleming, G. R. *Nature* **2007**, *446*, 782−786.
(6) Lee, H.; Cheng, Y.-C.; Fleming, G. R. *Science* **2007**, *316*, 1462−1465.
(7) Collini, E.; Wong, C. Y.; Wilk, K. E.; Curmi, P. M. G.; Brumer, P.; Scholes, G. D. *Nature* **2010**, *463*, 644−647.
(8) Ishizaki, A.; Calhoun, T. R.; Schlau-Cohen, G. S.; Fleming, G. R. *Phys. Chem. Chem. Phys.* **2010**, *12*, 7319−7337.
(9) Panitchayangkoon, G.; Hayes, D.; Fransted, K. A.; Caram, J. R.; Harel, E.; Wen, J.; Blankenship, R. E.; Engel, G. S. *Proc. Natl. Acad. Sci. U.S.A.* **2010**, *107*, 12766−12770.
(10) Scholes, G. D. *J. Phys. Chem. Lett.* **2010**, *1*, 2−8.
(11) Wong, C. Y.; Alvey, R. M.; Turner, D. B.; Wilk, K. E.; Bryant, D. A.; Curmi, P. M. G.; Silbey, R. J.; Scholes, G. D. *Nat. Chem.* **2012**, *4*, 396−404.
(12) Novoderezhkin, V.; Van Grondelle, R. *J. Phys. Chem. B* **2013**, *117*, 11076−11090.
(13) Renger, T. *Photosynth. Res.* **2009**, *102*, 471−485.
(14) Hsu, C. P.; Fleming, G. R.; Head-Gordon, M.; Head-Gordon, T. *J. Chem. Phys.* **2001**, *114*, 3065−3072.
(15) Iozzi, M. F.; Mennucci, B.; Tomasi, J.; Cammi, R. *J. Chem. Phys.* **2004**, *120*, 7029−7040.
(16) Hsu, C.-P. *Acc. Chem. Res.* **2009**, *42*, 509−518.
(17) Curutchet, C.; Munoz-Losa, A.; Monti, S.; Kongsted, J.; Scholes, G. D.; Mennucci, B. *J. Chem. Theory Comput.* **2009**, *5*, 1838−1848.
(18) Neugebauer, J.; Curutchet, C.; Munoz-Losa, A.; Mennucci, B. *J. Chem. Theory Comput.* **2010**, *6*, 1843−1851.
(19) Mennucci, B.; Curutchet, C. *Phys. Chem. Chem. Phys.* **2011**, *13*, 11538−11550.
(20) Novoderezhkin, V. I.; Van Grondelle, R. *Phys. Chem. Chem. Phys.* **2010**, *12*, 7352−7365.
(21) Janosi, L.; Kosztin, I.; Damjanovic, A. *J. Chem. Phys.* **2006**, *125*, 014903.
(22) Olbrich, C.; Kleinekathoefer, U. *J. Phys. Chem. B* **2010**, *114*, 12427−12437.
(23) Olbrich, C.; Jansen, T. L. C.; Liebers, J.; Aghtar, M.; Struempfer, J.; Schulten, K.; Knoester, J.; Kleinekathoefer, U. *J. Phys. Chem. B* **2011**, *115*, 8609−8621.
(24) Shim, S.; Rebentrost, P.; Valleau, S.; Aspuru-Guzik, A. *Biophys. J.* **2012**, *102*, 649−660.
(25) Curutchet, C.; Novoderezhkin, V. I.; Kongsted, J.; Munoz-Losa, A.; Van Grondelle, R.; Scholes, G. D.; Mennucci, B. *J. Phys. Chem. B* **2013**, *117*, 4263−4273.
(26) Müh, F.; Madjet, M. E.-A.; Adolphs, J.; Abdurahman, A.; Rabenstein, B.; Ishikita, H.; Knapp, E.-W.; Renger, T. *Proc. Natl. Acad. Sci. U.S.A.* **2007**, *104*, 16862−16867.
(27) Renger, T.; Müh, F. *Phys. Chem. Chem. Phys.* **2013**, *15*, 3348−3371.
(28) Schreiber, M.; Silva-Junior, M. R.; Sauer, S. P.; Thiel, W. *J. Chem. Phys.* **2008**, *128*, 134110.
(29) Silva-Junior, M. R.; Schreiber, M.; Sauer, S. P. A.; Thiel, W. *J. Chem. Phys.* **2008**, *129*, 104103.
(30) Jacquemin, D.; Wathelet, V.; Perpete, E. A.; Adamo, C. *J. Chem. Theory Comput.* **2009**, *5*, 2420−2435.
(31) Silva-Junior, M. R.; Thiel, W. *J. Chem. Theory Comput.* **2010**, *6*, 1546−1564.
(32) Caricato, M.; Trucks, G. W.; Frisch, M. J.; Wiberg, K. B. *J. Chem. Theory Comput.* **2010**, *6*, 370−383.
(33) Jacquemin, D.; Mennucci, B.; Adamo, C. *Phys. Chem. Chem. Phys.* **2011**, *13*, 16987−16998.
(34) Leang, S. S.; Zahariev, F.; Gordon, M. S. *J. Chem. Phys.* **2012**, *136*, 104101.
(35) Adamo, C.; Jacquemin, D. *Chem. Soc. Rev.* **2013**, *42*, 845−856.
(36) Linnanto, J.; Korppi-Tommola, J. *Phys. Chem. Chem. Phys.* **2006**, *8*, 663−687.
(37) Fenna, R. E.; Matthews, B. W. *Nature* **1975**, *258*, 573−577.
(38) Busch, M. S. A.; Müh, F.; Madjet, M. E.-A.; Renger, T. *J. Phys. Chem. Lett.* **2011**, *2*, 93−98.
(39) Viani, L.; Curutchet, C.; Mennucci, B. *J. Phys. Chem. Lett.* **2013**, *4*, 372−377.
(40) Parusel, A. B. J.; Grimme, S. *J. Phys. Chem. B* **2000**, *104*, 5395−5398.
(41) Balaban, T. S.; Braun, P.; Hättig, C.; Hellweg, A.; Kern, J.; Saenger, W.; Zouni. *Biochim. Biophys. Acta* **2009**, *1787*, 1254.
(42) Tronrud, D. E.; Wen, J.; Gay, L.; Blankenship, R. E. *Photosynth. Res.* **2009**, *100*, 79−87.

(43) *Schrödinger Suite 2011 Protein Preparation Wizard; Epik*, version 2.2; Schrödinger, LLC: New York, 2011; *Impact*, version 5.7; Schrödinger, LLC: New York, 2011; *Prime*, version 3.0; Schrödinger, LLC: New York, 2011.
(44) Sastry, G. M.; Adzhigirey, M.; Day, T.; Annabhimoju, R.; Sherman, W. *J. Comput. Aided Mol. Des.* **2013**, *27*, 221−234.
(45) *Prime, version 3.0*; Schrödinger, LLC: New York, 2011.
(46) Jacobson, M. P.; Friesner, R. A.; Xiang, Z.; Honig, B. *J. Mol. Biol.* **2002**, *320*, 597−608.
(47) Jacobson, M. P.; Pincus, D. L.; Rapp, C. S.; Day, T. J. F.; Honig, B.; Shaw, D. E.; Friesner, R. A. *Proteins: Struct., Funct., Bioinf.* **2004**, *55*, 351−367.
(48) Kaminski, G. A.; Friesner, R. A.; Tirado-Rives, J.; Jorgensen, W. L. *J. Phys. Chem. B* **2001**, *105*, 6474−6487.
(49) *QSite*, version 5.7; Schrödinger, LLC, New York, 2011.
(50) Murphy, R. B.; Philipp, D. M.; Friesner, R. A. *J. Comput. Chem.* **2000**, *21*, 1442−1457.
(51) Philipp, D. M.; Friesner, R. A. *J. Comput. Chem.* **1999**, *20*, 1468−1494.
(52) Becke, A. D. *J. Chem. Phys.* **1993**, *98*, 5648.
(53) Vosko, S. H.; Wilk, L.; Nusair, M. *Can. J. Phys.* **1980**, *58*, 1200−1211.
(54) Stephens, P. J.; Devlin, F. J.; Chabalowski, C. F.; Frisch, M. J. *J. Phys. Chem.* **1994**, *98*, 11623−11627.
(55) Lee, C.; W., Y.; Parr, R. G. *Phys. Rev. B.* **1988**, *37*, 785−789.
(56) Hay, P. J.; Wadt, W. R. *J. Chem. Phys.* **1985**, *82*, 299.
(57) Hehre, W. J.; Ditchfield, R.; Pople, J. A. *J. Chem. Phys.* **1972**, *56*, 2257.
(58) Hariharan, P. C.; Pople, J. A. *Theor. Chim. Acta* **1973**, *28*, 213−222.
(59) Grimme, S.; Waletzke, M. *J. Chem. Phys.* **1999**, *111*, 5645−5655.
(60) Kleinschmidt, M.; Marian, C. M.; Waletzke, M.; Grimme, S. *J. Chem. Phys.* **2009**, *130*, 044708.
(61) Weigend, F.; Ahlrichs, R. *Phys. Chem. Chem. Phys.* **2005**, *7*, 3297−3305.
(62) Lee, C.; Yang, W.; Parr, R. G. *Phys. Rev. B* **1988**, *37*, 785−789.
(63) Becke, A. D. *J. Chem. Phys.* **1993**, *98*, 1372−1377.
(64) TURBOMOLE V6.3 2011, a development of University of Karlsruhe and Forschungszentrum Karlsruhe GmbH, 1989−2007, TURBOMOLE GmbH, since 2007; available via the Internet athttp://www.turbomole.com.
(65) Christiansen, O.; Koch, H.; Jørgensen, P. *Chem. Phys. Lett.* **1995**, *243*, 409−418.
(66) Hättig, C.; Weigend, F. *J. Chem. Phys.* **2000**, *113*, 5154.
(67) Janssen, C. L.; Nielsen, I. *Chem. Phys. Lett.* **1998**, *290*, 423−430.
(68) Frisch, M. J.et al. *Gaussian 09, Revision A.1*; Gaussian, Inc.: Wallingford, CT, 2009.
(69) Zerner, M. C. *Rev. Comput. Chem.* **1991**, *2*, 313−365.
(70) Becke, A. D. *Phys. Rev. A* **1988**, *38*, 3098−3100.
(71) Perdew, J. P.; Burke, K.; Ernzerhof, M. *Phys. Rev. Lett.* **1996**, *77*, 3865−3868.
(72) Adamo, C.; Barone, V. *J. Chem. Phys.* **1999**, *110*, 6158−6170.
(73) Yanai, T.; Tew, D. P.; Handy, N. C. *Chem. Phys. Lett.* **2004**, *393*, 51−57.
(74) Tatchen, J.; Kleinschmidt, M.; Marian, C. M. *J. Photochem. Photobiol. A* **2004**, *167*, 201−212.
(75) Perun, S.; Tatchen, J.; Marian, C. M. *ChemPhysChem* **2008**, *9*, 282−292.
(76) Marian, C. M.; Gilka, N. *J. Chem. Theory Comput.* **2008**, *4*, 1501−1515.
(77) Louwe, R. J. W.; Vrieze, J.; Hoff, A. J.; Aartsma, T. J. *J. Phys. Chem. B* **1997**, *101*, 11280−11287.
(78) König, C.; Neugebauer, J. *J. Chem. Theory Comput.* **2013**, *9*, 1808−1820.
(79) Köhn, A.; Hättig, C. *J. Chem. Phys.* **2003**, *119*, 5021.
(80) Oviedo, M. B.; Sanchez, C. *J. Phys. Chem. A* **2011**, *115*, 12280−12285.
(81) Gudowska-Nowak, E.; Newton, M. D.; Fajer, J. *J. Phys. Chem.* **1990**, *94*, 5795−5801.
(82) Adolphs, J.; Renger, T. *Biophys. J.* **2006**, *91*, 2778−2797.
(83) Alden, R. G.; Johnson, E.; Nagarajan, V.; Parson, W. W.; Law, C. J.; Cogdell, R. G. *J. Phys. Chem. B* **1997**, *101*, 4667−4680.
(84) Scherz, A.; Parson, W. W. *Biochim. Biophys. Acta* **1984**, *766*, 653−665.
(85) Becker, M.; Nagarajan, V.; Parson, W. W. *J. Am. Chem. Soc.* **1991**, *113*, 6840−6848.
(86) Knox, R. S.; Spring, B. Q. *Photochem. Photobiol.* **2003**, *77*, 497−501.
(87) Knox, R. S. *Photochem. Photobiol.* **2003**, *77*, 492−496.
(88) Munoz-Losa, A.; Curutchet, C.; Galván, I. F.; Mennucci, B. *J. Chem. Phys.* **2008**, *129*, 034104.
(89) Rätsep, M.; Cai, Z.-L.; Reimers, J. R.; Freiberg, A. *J. Chem. Phys.* **2011**, *134*, 024506.
(90) Linnanto, J.; Korppi-Tommola, J. *J. Phys. Chem. A* **2004**, *108*, 5872−5882.
(91) Milder, M. T. W.; Brueggemann, B.; Van Grondelle, R.; Herek, J. L. *Photosynth. Res.* **2010**, *104*, 257−274.
(92) Louwe, R. J. W.; Vrieze, J.; Hoff, A. J.; Aartsma, T. J. *J. Phys. Chem. B* **1997**, *101*, 11280−11287.